The Cryosphere Discuss., 9, 115–140, 2015
www.the-cryosphere-discuss.net/9/115/2015/
doi:10.5194/tcd-9-115-2015

The Cryosphere Discussions
Open Access

Future projections of the climate and surface mass balance of Svalbard with the regional climate model MAR

C. Lang, X. Fettweis, and M. Erpicum

Département de Géographie, Université de Liège, Liège, Belgium

Received: 29 October 2014 – Accepted: 3 December 2014 – Published: 8 January 2015

Correspondence to: C. Lang (charlotte.lang@ulg.ac.be)

Published by Copernicus Publications on behalf of the European Geosciences Union.

Abstract

We have performed future projections of the climate and surface mass balance (SMB) of Svalbard with the MAR regional climate model forced by the MIROC5 global model, following the RCP8.5 scenario at a spatial resolution of 10 km. MAR predicts a similar evolution of increasing surface melt everywhere in Svalbard followed by a sudden acceleration of the melt around 2050, with a larger melt increase in the south compared to the north of the archipelago and the ice caps. This melt acceleration around 2050 is mainly driven by the albedo-melt feedback associated with the expansion of the ablation/bare ice zone. This effect is dampened in part as the solar radiation itself is projected to decrease due to cloudiness increase. The near-surface temperature is projected to increase more in winter than in summer as the temperature is already close to 0 °C in summer. The model also projects a strong winter west-to-east temperature gradient, related to the large decrease of sea ice cover around Svalbard. At the end of the century (2070–2099 mean), SMB is projected to be negative over the entire Svalbard and, by 2085, all glaciated regions of Svalbard are predicted to undergo net ablation, meaning that, under the RCP8.5 scenario, all the glaciers and ice caps are predicted to start their irreversible retreat before the end of the 21st century.

1 Introduction

Worldwide, glaciers and ice caps are observed to retreat. At present, they contribute to sea level rise (SLR) as much as the Antarctic and Greenland ice sheets (Gardner et al., 2013; Shepherd et al., 2012) and Arctic glaciers have been the second contributor to SLR among glaciers and ice caps between 1961 and 2004 (Kaser et al., 2006). However, contrary to what was previously estimated (Meier et al., 2007; Meehl et al., 2007), glaciers and ice caps (as found over Svalbard for example) are no longer believed to be the dominant contributors to SLR in the next decades, as the melt of the Antarctic and Greenland ice sheets has been accelerating (Rignot et al., 2011, 2014). Yet, the van-

TCD
9, 115–140, 2015

ishing of Svalbard glaciers could have huge impacts on the fauna and flora, permafrost (Isaksen et al., 2007; Etzelmüller et al., 2011), tourism and even possibly the development of agriculture, despite its low contribution to the sea level rise. Future projections of the Svalbard climate have been made (Førland et al., 2011) but the future evolution of the glaciers of Svalbard themselves have been little studied. Day et al. (2012) have studied the impact of the future sea ice decline on the temperature, precipitation and surface mass balance (SMB) of Svalbard while Radić and Hock (2011), Marzeion et al. (2012) and Radić et al. (2014) have evaluated the contribution of Svalbard glaciers to future sea level rise. However, these SMB calculations are based on empirical models and are rarely forced by outputs from high resolution atmospheric models but rather by global ones. That is why we propose a more extensive study at high resolution of the future of Svalbard glaciers and ice caps using the regional climate model MAR (Modèle Atmosphérique Régional) evaluated over the current Svalbard climate in the companion paper Lang et al. (2014). Compared to previously published future projections, MAR allows us to perform future projections of the surface mass balance by explicitly taking into account the atmosphere-surface feedbacks, as it is fully coupled to an energy balance snow model. In this study, MAR has been forced by the general circulation model MIROC5 (Model for Interdisciplinary Research on Climate) to perform future projections of the climate and SMB over Svalbard based on the RCP8.5 scenario ($MAR_{RCP8.5}$). MAR forced by MIROC5 over current climate (MAR_{histo}) has been successfully evaluated over Svalbard by Lang et al. (2014). Section 2 contains a brief description of the models and the set-ups. In Sect. 3, we present the future SMB of Svalbard and its regional evolution through the 21st century. In Sect. 4, we investigate the temperature change and how it should be impacted by the sea ice cover decrease. In Sect. 5, we describe the evolution of the melt season and, finally, the sensitivity of the energy balance components to rising temperatures is investigated in Sect. 6 before concluding in Sect. 7.

TCD
9, 115–140, 2015

2 Models and forcings

MAR (Gallée and Schayes, 1994) is a regional climate atmospheric model fully coupled to a surface model resolving the energy balance at the surface of the snow pack and has been described in Lang et al. (2014). The version and forcings of the model are the same as those used over the present era in Lang et al. (2014). We have run MAR over the period 2006–2100 at a spatial resolution of 10 km. The lateral and upper (tropopause) boundaries (temperature, humidity, wind speed and surface pressure) as well as oceanic boundaries (sea surface temperature and sea ice cover) were forced every 6 h by the MIROC5 global model using the RCP8.5 scenario (Watanabe et al., 2010; Sakamoto et al., 2012).

3 Surface mass balance

Figure 1a shows that MAR-based SMB is projected to be negative on average over 2070–2099 over the entire archipelago, according to the MIROC5-based RCP8.5 scenario. $MAR_{RCP8.5}$ predicts that the greatest losses will mostly happen in the southern part of Spitsbergen with values going from −3000 up to −6000 mm w.e. yr^{-1} in the most extreme cases, where we also have the greatest differences compared to the 1980–2005 average (Fig. 1b and Supplement Fig. S1 for MAR_{histo} SMB). This suggests that the surface mass loss from small southern glaciers will be higher than over the ice caps and large ice fields of northern Spitsbergen. The mean 2070–2099 meltwater runoff anomaly is largely positive (Fig. 1c) and the largest anomalies (> 5000 mm w.e. yr^{-1}) are also located in the south of the archipelago. The snowfall accumulation will mostly increase (Fig. 1d) but far from enough to compensate for the increase in meltwater runoff, as also simulated by MAR over the Greenland ice sheet (Fettweis et al., 2013) and by RACMO2 in the Canadian Arctic Archipelago (Lenaerts et al., 2013). Along the coastline however, the snowfall anomaly is negative, because the winter solid precip-

TCD
9, 115–140, 2015

itation increase will not be able to compensate for the summer decrease, as a large part of the current snowfall should become rainfall at the end of this century.

Figure 2, showing the temporal evolution of the annual SMB for the 5 different regions presented in the inset, confirms that the surface mass loss acceleration after 2050 is larger in the south of the archipelago than in the north.

$MAR_{RCP8.5}$ and MAR_{histo} project a similar SMB evolution for all our 5 regions until 2050. After 2050, the acceleration of surface mass loss is projected to increase suddenly and be more pronounced in the south of Spitsbergen and on Barentsøya and Edgeøya (BE) than in west/east Spitsbergen and on Austfonna and Vestfonna (AV). After 2085, the surface mass loss is projected to stabilize and even to decrease a bit according to the MIROC5-based RCP85 scenario. The SMB future evolution is in a vast majority driven by the significant runoff increase and, to a lesser extent, by the snowfall accumulation increase (Fig. 3a and b). For example, the SMB evolution of east Spitsbergen and the AV ice caps is almost identical while the runoff evolution is different. However, the snowfall, heavier in the East than on AV, compensates for the higher runoff rates in the East, resulting in almost equal SMB over both regions.

The increasing summer (JJA for June-July-August) near-surface temperature (TAS_{JJA}) explains in part the melt increase but not the acceleration of melt around 2050 (Fig. S2a), resulting rather from the surface JJA albedo-melt feedback associated with the expansion of the ablation/bare ice zone as also projected over the Greenland ice sheet (Franco et al., 2013). However, the melt-JJA albedo feedback (Fig. 3c) is partly reduced in the West by the decrease of the solar flux caused by a larger cloud cover in west and south Spitsbergen in summer, compared to the northeast and the AV ice caps (Fig. S2b and c). The larger cloud cover in the West and the South is caused by a warmer and therefore more humid atmosphere and higher evaporation due to the lower sea ice cover in summer. As a result, despite a larger decrease of JJA surface albedo in west Spitsbergen than in the other northern regions, the amount of net shortwave radiation available for the melt in summer (SWDnet, see Eq. 1 in Sect. 6) in west Spitsbergen is closer to the amount of JJA SWDnet over the other northern regions

TCD
9, 115–140, 2015

(Fig. 3d). Note that for consistency, the summer values have been considered here over June-July-August only but, at the end of the century, the melt season will cover a much longer period (see Sect. 5). As a consequence, some minor differences appear between SMB or melt curves and the energy fluxes but the main feature, i.e. the larger acceleration in the South, is well visible on the graph.

Figure 4 shows the projected anomaly of the surface ice loss over the 21st century with respect to the Historical mean (1980–2005). In the South and along the west coast, some glaciers could lose more than 200 m of ice. Note that we consider here the thickness in metres of ice (920 kg m^{-3}) and did not convert it in water equivalent. On BE, the accumulation zone could disappear (Fig. 3e) as soon as 2035, according to MIROC5-based RCP8.5 scenario, meaning that, after that, there will not be any mass gain anymore in the centre of the ice cap to compensate for the mass loss at the margins and all the permanent snow/ice will probably disappear by the end of the century.

On Austfonna on the contrary, given the large ice thickness (Dowdeswell et al., 2008), we expect that, under RCP8.5 scenario, a great part (in area) of the ice cap will remain at the end of the century and that the retreat will only concern the margins. However, as $MAR_{RCP8.5}$ predicts a negative SMB over both Austfonna and Vestfonna by 2085, the ice caps is still projected to start its irreversible retreat at the end of this century.

Over the whole 21st century, the integrated Svalbard $MAR_{RCP8.5}$ based SMB decrease corresponds to a difference of −2600 km^3 w.e. (i.e. −2827 km^3 of ice) with respect to the Historical mean, contributing for 7.2 mm to the 21st century sea level rise (SLR), according to MIROC5-based $MAR_{RCP8.5}$. Radić et al. (2014) calculated a mean value of the sea level rise associated with the 21st century SMB changes of Svalbard with a Positive Degree-Day (PDD) model based on the outputs of an ensemble of 14 GCMs for the RCP8.5 scenario. Their projected SLR at the end of the century is more than twice as large as ours (15.81 mm). Marzeion et al. (2012) projected a SLR between 15 and 25 mm for Svalbard, with an empirical model based on the outputs of climatologies and CMIP5 GCMs. However, these values were based on large scale

TCD
9, 115–140, 2015

temperature and precipitation changes from global models in most of which Svalbard is not explicitly represented given their huge spatial resolution. Therefore, it is very likely that the snowfall increase with rising temperature is not taken into account by GCMs. Radić et al. (2014) estimated the total present ice volume of Svalbard to be 9089 km^3, which corresponds to a potential sea level rise of 23 mm. Our projections therefore suggests that 31 % of their present estimated volume will disappear by 2100. According to a previous estimate of 7000 km^3 (equivalent to a sea level rise of 20 mm) by Hagen et al. (1993), about 40 % of the ice mass is projected to disappear by 2100 in our projections, due to surface mass loss only.

As shown in Lang et al. (2014), a resolution of 10 km smoothens the topography, especially on Spitsbergen where the topography is very steep. As a result, the elevation is underestimated over a large part of Svalbard and some low altitude glaciers should not even exist in our 10 km grid, causing a likely overestimation of the surface mass loss in our projections. Moreover, the topography and ice mask are also fixed in our simulations, which is an acceptable approximation under the present climate but will likely introduce an underestimation of the melt increase in the future, as a result of glaciers thinning. As the glaciers and ice caps thin, the surface elevation decreases, inducing an additional warming and therefore melt. Keeping a fixed topography in our simulation therefore underestimates the acceleration of melt through the 21st century. On the other hand, glaciers are going to retreat in the future and using a fixed ice mask overestimates the melt increase once integrated over large areas, as some areas should not be covered with permanent ice under the future warmer climate and the contribution of these areas (with huge projected melt increase) to the sea level rise should be removed in our projections. However, by the end of the century, we expect those three effects to compensate each other and to not impact a lot our future projections. Indeed, over the Greenland ice sheet, those effects are projected to contribute to about only 5–10 % of the SMB anomaly (Fettweis et al., 2013) and we expect their contribution to be of the same order of magnitude in Svalbard. However, only a high resolution simulation coupled with an ice sheet model could evaluate precisely this con-

TCD
9, 115–140, 2015

tribution. In south Spitsbergen, given the very negative values of SMB and the fact that we have glaciers rather than ice caps, we expect the retreat effect to be dominant and $MAR_{RCP8.5}$ probably overestimates the surface mass loss in this area. On Austfonna, on the other hand, we expect the retreat to be limited only to the proximity of the margins but the elevation decrease towards the centre of the ice cap is also expected to be limited. We therefore expect that both effects will balance each other, or at least that none of them will be largely dominant. But, again, the only way to be certain of that is to run a MAR simulation coupled with an ice sheet model.

4 Near-surface temperature

$MAR_{RCP8.5}$ predicts a rather small and spatially homogeneous JJA near-surface temperature (TAS) increase (3.5 to 6.5 °C) compared to the DJF (December-January-February) increase, much larger (11 to 25 °C, Figs. 5 and 7a) and displaying a 10-degree west-to-east gradient over Svalbard. The pattern and magnitude of the temperature increase modelled by $MAR_{RCP8.5}$ are similar to Day et al. (2012) estimates. Førland et al. (2011) projected a temperature increase in Longyearbyen of 3.3 and 11.9 °C in JJA and DJF by the end of the century using B2, A1B and A2 scenarios while our temperature is projected to increase by 6 °C in JJA and 14 °C in DJF. Considering that Day et al. (2012) and Førland et al. (2011) worked with B2, A1B and A2 scenarios and we used RCP8.5, it is normal that our temperature increase is a little bit larger (Rogelj et al., 2012) and we can conclude that our results are comparable to those of Day et al. (2012) and Førland et al. (2011).

In summer, TAS is already close to 0 °C over the Historical period (Fig. S3a) and can not increase very much because the excess energy available at the surface is used to melt snow/ice. According to MIROC5-based RCP8.5 scenario, JJA temperature is projected to increase by 3.75 to 4.75 °C over the glaciated areas (Fig. 5a) and the only regions where the TAS increase is larger (up to 6.5 °C) are regions with small

TCD
9, 115–140, 2015

permanent ice area at present, i.e. BE and Nordenskiöld Land (orange area separating the north and south of Svalbard in Fig. 5a).

The higher temperature increase in winter is due to (i) very low present-day DJF temperatures (Fig. S3b) allowing it to increase much more before reaching freezing point and (ii) the projected decrease of the winter sea ice cover (SIC) (also highlighted by Day et al., 2012 and Førland et al., 2011), that is also responsible for the large west-to-east temperature gradient. At present, there is a large west-to-east SIC gradient as the North Atlantic Drift prevents sea ice to form west of Svalbard as much as in the East, which is largely covered with sea ice. With the projected temperatures increasing, the sea ice will start to not form and, due to a positive feedback, the ocean surface will be warmer, which in turn will warm the near surface atmosphere over Svalbard, which will enhance the sea ice formation decrease furthermore. In the future, near-surface temperature will increase more where there is a possibility for more sea ice extent to decrease. Therefore, in the West, as there is already no significant sea ice cover in the present climate, SIC/temperature contrast with our future projections is much lower than in the East. We have shown in Lang et al. (2014) that the ocean has a large influence on Svalbard, even quite far inland. In Fig. S3a, showing the 1980–2005 mean JJA TAS, the temperature follows the altitude whereas in winter (Fig. S2b), the only temperature gradient is the west-to-east gradient due to the presence or absence of sea ice. At the end of the century, the altitude gradient is projected to become dominant in winter (Fig. S3b) as most of the sea ice should have disappeared according to the MIROC5-based RCP8.5 scenario. Finally, the DJF east coast maximum temperature increase in Day et al. (2012) is located on the east coast of Nordaustlandet whereas our is on BE and our Nordaustlandet anomaly rather lies around +16/17 °C, compared to +21 °C in Day et al. (2012) using HadRM3. This is probably due to the fact that MIROC5 overestimates the present sea ice extent and still has up to 40 % of sea ice cover on the east coast of Nordaustlandet over the period 2070–2099 (Fig. S5) whereas HadGEM1's ocean is mostly ice-free at the end of this century.

TCD
9, 115–140, 2015

5 Melt season

During the first half of this century, $MAR_{RCP8.5}$ projects that the beginning of the melt season (Fig. 6a) will not vary much (melt season will start 0.2 day sooner per year) because the effect of the temperature increase bringing more energy for the melt (Fig. 7a) will be compensated by the albedo effect (Fig. 7c) induced by increasing winter snowfall accumulation (Fig. 7b). As the amount of snowfall increases, so does the winter snowpack height above bare ice/old dirty snow at the beginning of the summer. The appearance of low albedo zones in summer is therefore delayed and SWDnet available for the melt in the energy budget is reduced. After the 2050s, the temperature increase is projected to overcome the effect of heavier snowfall accumulation and the melt season is expected to start significantly sooner (1.5 day sooner per year).

The seasonal maximum of melt happens around 15–20 July through the whole 21st century, at the same time as the temperature maximum. Before 2050, the temperature seasonal cycle is more or less symmetrical with respect to its maximum value. On the other hand, we have a maximum of solid precipitation in fall. The melt (resp. albedo) seasonal cycle is also symmetrical with respect to its maximum (resp. minimum) (Figs. 6b and 7c). In the second half of the century, the temperature and therefore the melt are projected to increase more after their seasonal maximum than at the beginning of summer. The melt asymmetry is also partly explained by the changes of snowfall accumulation which are projected to increase before June but to significantly decrease in late summer, impacting the melt through the positive albedo feedback.

As soon as the 2030s, $MAR_{RCP8.5}$ does not simulate any delay between the maximum of melt and the maximum of runoff anymore (Fig. 6d, e and f). The 5 to 8 days delay visible on Fig. 6d, e and f corresponds to the time needed in MAR for the meltwater to runoff from the glaciers to the sea (Zuo and Oerlemans, 1996; Lefebre et al., 2002). The maximum of runoff is also projected to be equal (or almost) to the maximum of melt. This concordance in time is due to the fact that, from the 2030s, at the time of the maximum of melt, the melting area is no longer covered with melting snow (retaining

TCD
9, 115–140, 2015

part of the meltwater and delaying the runoff) but rather with bare ice or impermeable snowpack damping the meltwater retention capacity of the glaciers. During the Historical period and until the 2020s on the other hand, the presence of snow above ice in the ablation zone allows part of meltwater to be stored in the snowpack and refreeze in winter without running off. Conversely, at the beginning of the melt season, there is still a small delay between the melt and runoff seasons as the bare ice is covered by the winter snowpack even at the end of the century. However, this delay will decrease more steadily with time, as the water storage and refreezing capacity will also decrease, as a consequence of the snow cover decrease in the enlarging ablation zone.

6 Energy balance

Studying energy balance components anomaly vs. temperature anomaly (rather than vs. time) offers the advantage of less dependance on a particular future scenario as shown by Fettweis et al. (2013). Figure 8b shows that the JJA net energy flux at the surface (and therefore melt and runoff, Fig. 8a) quadratically increase with the JJA TAS projected changes, as also projected over Greenland (Franco et al., 2013).

The net energy available at the surface for the melt (NET) can be calculated as follow:

$$\mathrm{NET} = \mathrm{SWDnet} + \mathrm{LWnet} + \mathrm{SHF} + \mathrm{LHF} \quad (\mathrm{W\,m^{-2}}) \tag{1}$$

where

- SWDnet = SWD × (1 – a) is the net downward shortwave radiation, i.e. the amount of the downward shortwave (= solar radiation) energy flux (SWD) that is absorbed by the surface following its albedo (a).
- LWnet = LWD – LWU is the net longwave radiation, i.e., the difference between the downward longwave radiation coming from the atmosphere and the upward longwave radiation emitted by the surface.

TCD
9, 115–140, 2015

– SHF and LHF are the sensible and latent heat fluxes.

Figure 8c shows the evolution of the anomaly of each energy balance component (JJA) as a function of the TAS_{JJA} anomaly. In order to distinguish the albedo and solar radiation effects in SWDnet, we have considered two variables for the net solar radiation, as done in Franco et al. (2013). First, we kept the albedo value constant (by using the 1980–2005 mean value) and allowed only SWD to vary (SWDswd). Secondly, we kept the SWD value constant and allowed only the albedo to vary (SWDalb).

$MAR_{RCP8.5}$ predicts that, at the end of the century (2080–2099 mean), the anomaly of SWDnet will represent 33 % of the NET anomaly while the SWDalb anomaly, reflecting the effect of the albedo on SWDnet, will count for 50 % of the NET anomaly (Supplement Table S1). The expected increase in cloud cover will decrease the incident solar radiation at the surface (SWDswd, Fig. 8c) and be opposed to the increase of SWDalb associated with the decreasing albedo but will not be large enough to contrebalance it, leading to a positive and increasing SWDnet, as also projected over Greenland (Franco et al., 2013).

The second largest contribution to the NET increase is the sensible heat flux, whose anomaly at the end of the century is projected to represent 24 % of the NET anomaly, as a consequence of the advection of warmer (oceanic) air over the cold ice/snow surface. At present, the modelled TAS is negative on average in summer and therefore lower than the snow/ice temperature (0 °C as the surface snow/ice is melting). SHF is thus also negative and the surface loses energy to the atmosphere. $MAR_{RCP8.5}$ predicts that, around 2030, the summer near-surface temperature will become positive and consequently higher than the melting snow/ice temperature. The JJA SHF averaged over the entire Svalbard will also become positive and the atmosphere will give energy to the surface on average. The third contribution to the NET change is the latent heat flux, counting for 22 % over Svalbard, whereas it is the smallest contributor of the energy fluxes over Greenland (Franco et al., 2013). LHF is currently negative as evaporation and sublimation, requiring energy, are the dominant processes but they will decrease in the future in favour of condensation and deposition (giving energy to

TCD
9, 115–140, 2015

the surface, hence a positive value of LHF) as more and more humid and warm air due to the reduction of sea ice during summer will be advected towards the cold ice surface. On the other hand, condensation and deposition will also directly contribute to accumulation (10 % of the mean 2080–2099 accumulation) and act in opposition to the LHF effect on the melt. In contrast to the Greenland ice sheet (Noël et al., 2014), which is higher in altitude, the oceanic conditions around Svalbard impact a lot on its climate. In Svalbard, the katabatic winds, weaker than in Greenland, can not prevent the warm oceanic air to penetrate up to the central regions and the SHF and LHF increase will take place over the entire land area instead of along the ice sheet margins as in Greenland (Franco et al., 2013).

Finally, the last contribution will come from the net longwave radiation flux (LWnet, 21 % of the 2080–2099 NET anomaly). The increase in longwave radiation emitted downward by the warmer and wetter atmosphere following the increase of the greenhouse gases concentration should partly be contrebalanced by the increase in upward longwave radiation emitted by the surface, due to the surface temperature increase.

7 Conclusions

Over the 21st century, according to $MAR_{RCP8.5}$, the snow/ice albedo feedback related to the extension of the ablation zone area will drive the evolution of the SMB through the net shortwave radiation absorbed by the surface and available for the melt in the enregy budget. Around 2060, the mass loss coming from the surface melt increase is projected to accelerate and $MAR_{RCP8.5}$ simulates a larger acceleration of the mass loss in the south of the archipelago compared to the north, due to a larger increase of JJA SWDnet in the South, itself due to the larger decrease of the JJA surface albedo in the South than in the North. SWDnet is the component of the energy balance the most sensitive to an increase in temperature because of the decreasing surface albedo. However, the downward shortwave radiation itself should decrease with increasing temperature due

TCD
9, 115–140, 2015

to an increase in cloudiness and partly countrebalance the effect of the melt-albedo positive feedback.

The summer sensible and latent heat fluxes, that are both negative at present, will increase with increasing temperature and become positive in the future and give energy to the surface. The LHF increase will be caused by the decreasing SIC allowing more evaporation around Svalbard and warmer and more humid air to be advected on the cold ice surface, showing that the oceanic conditions impacts Svalbard a lot, even far inland. The SHF will become positive when the temperature of the warmer oceanic air advected over the cold ice/snow surface will become positive, causing the atmosphere to give energy to the surface.

The temperature is projected to increase more in winter than in summer and there should be a strong winter west-to-east temperature gradient. These two features are related to the large decrease of sea ice cover in accordance with Day et al. (2012) and Førland et al. (2011). The decreasing SIC will therefore also contribute to the melt increase in addition to contributing to the turbulent fluxes increase through its effect on the near-surface temperature.

All glaciated areas of the archipelago are projected to undergo net ablation by the end of the century. The disappearance of the accumulation zone should happen much earlier in the south and northwest of Spitsbergen than in the northeast and on the ice caps. But, even in these areas, the permanent ice zones are expected to start to irreversibly disappear by the end of the century. Svalbard 21st century contribution to sea level rise under the RCP8.5 scenario will be about 7.1 mm, according to MIROC5-based MAR.

The increase of snowfall accumulation during winter and spring and the small increase in temperature at the beginning of the melt season explain why, during the first half of this century, the melt season is not expected to start much earlier than now, as the low albedo zones will be covered by a thicker winter snowpack. However, as the melt area is projected to be no longer covered with melting snow but rather with bare ice as soon as the 2030s, the meltwater retention capacity of the ice sheet should

TCD
9, 115–140, 2015

decrease a lot and the maximum of runoff should be equal to the maximum of melt and there should not be any delay between them quite rapidly.

Finally, it should be noted that the ice caps topography is fixed during our simulation, suggesting that we underestimate the surface mass loss in our projections as glacier thinning is not taken into account. On the other hand, our ice sheet mask is also fixed, suggesting that our projected integrated surface melt include ice areas that could disappear in the near future and therefore that we could overestimate the contribution of Svalbard to the sea level rise. This motivates the necessity to couple MAR with an ice sheet model in further developments to evaluate if not taking into account the glaciers thinning is counterbalanced by the use of a fixed permanent ice mask or not. In addition, future projections at higher resolution (~ 5 km) are required to better resolve the altitude of small glaciers.

The Supplement related to this article is available online at doi:10.5194/tcd-9-115-2015-supplement.

Acknowledgements. C. Lang works under a PhD grant from the Fonds pour la formation à la Recherche dans l'Industrie et l'Agriculture (FRIA), Belgium.

References

Day, J. J., Bamber, J. L., Valdes, P. J., and Kohler, J.: The impact of a seasonally ice free Arctic Ocean on the temperature, precipitation and surface mass balance of Svalbard, The Cryosphere, 6, 35–50, doi:10.5194/tc-6-35-2012, 2012. 117, 122, 123, 128

Dowdeswell, J. A., Benham, T. J., Strozzi, T., and Hagen, J. O.: Iceberg calving flux and mass balance of the Austfonna ice cap on Nordaustlandet, Svalbard, J. Geophys. Res., 113, F03022, doi:10.1029/2007JF000905, 2008. 120

TCD
9, 115–140, 2015

Etzelmüller, B., Schuler, T. V., Isaksen, K., Christiansen, H. H., Farbrot, H., and Benestad, R.: Modeling the temperature evolution of Svalbard permafrost during the 20th and 21st century, The Cryosphere, 5, 67–79, doi:10.5194/tc-5-67-2011, 2011. 117

Fettweis, X., Franco, B., Tedesco, M., van Angelen, J. H., Lenaerts, J. T. M., van den Broeke, M. R., and Gallée, H.: Estimating the Greenland ice sheet surface mass balance contribution to future sea level rise using the regional atmospheric climate model MAR, The Cryosphere, 7, 469–489, doi:10.5194/tc-7-469-2013, 2013. 118, 121, 125

Førland, E. J., Benestad, R., Hanssen-Bauer, I., Haugen, J. E., and Skaugen, T. E. : Temperature and precipitation development at Svalbard 1900–2100, Adv. Meteorol., 2011, 893790, doi:10.1155/2011/893790, 2011. 117, 122, 123, 128

Franco, B., Fettweis, X., and Erpicum, M.: Future projections of the Greenland ice sheet energy balance driving the surface melt, The Cryosphere, 7, 1–18, doi:10.5194/tc-7-1-2013, 2013. 119, 125, 126, 127

Gallée, H. and Schayes, G.: Development of a three-dimensional meso-γ primitive equation model: katabatic winds simulation in the area of Terra Nova Bay, Antarctica, Mon. Weather Rev., 122, 671–685, 1994. 118

Gardner, A. S., Moholdt, G., Cogley, J. G., Wouters, B., Arendt, A. A., Wahr, J., Berthier, E., Hock, R., Pfeffer, W. T., Kaser, G., Ligtenberg, S. R. M., Bolch, T., Sharp, M. J., Hagen, J. O., van den Broeke, M. R., and Paul, F.: A reconciled estimate of glacier contributions to sea level rise: 2003 to 2009, Science, 340, 852–857, 2013. 116

Hagen, J. O., Liestøl, O., Roland, E., and Jørgensen., T.: Glacier Atlas of Svalbard and Jan Mayen, Norwegian Polar Institue, Oslo, 1993. 121

Isaksen, K., Benestad, R. E., Harris, C., and Sollid, J. L.: Recent extreme near-surface permafrost temperatures on Svalbard in relation to future climate scenarios, Geophys. Res. Lett., 34, L17502, doi:10.1029/2007GL031002, 2007. 117

Kaser, G., Cogley, J. G., Dyurgerov, M. B., Meier, M. F., and Ohmura, A.: Mass balance of glaciers and ice caps: consensus estimates for 1961–2004, Geophys. Res. Lett., 33, L19501, doi:10.1029/2006GL027511, 2006. 116

Lang, C., Fettweis, X., and Erpicum, M.: Stable climate and surface mass balance in Svalbard over 1979–2013 despite the Arctic warming, The Cryosphere Discuss., 8, 4497–4543, doi:10.5194/tcd-8-4497-2014, 2014. 117, 118, 121, 123, 133

TCD
9, 115–140, 2015

Lefebre, F., Gallée, H., van Yperzele, J.-P., and Huybrechts, P.: Modelling of large-scale melt parameters with a regional climate model in south Greenland during the 1991 melt season, Ann. Glaciol., 35, 391–397, 2002. 124

Lenaerts, J. T. M., van Angelen, J. H., van den Broeke, M. R., Gardner, A. S., Wouters, B., and van Meijgaard, E.: Irreversible mass loss of Canadian Arctic Archipelago glaciers, Geophys. Res. Lett., 40, 870–874, doi:10.1002/grl.50214, 2013. 118

Marzeion, B., Jarosch, A. H., and Hofer, M.: Past and future sea-level change from the surface mass balance of glaciers, The Cryosphere, 6, 1295–1322, doi:10.5194/tc-6-1295-2012, 2012. 117, 120

Meehl, G. A., Stocker, T. F., Collins, W. D., Friedlingstein, P., Gaye, A. T., Gregory, J. M., Kitoh, A., Knutti, R., Murphy, J. M., Noda, A., Raper, S. C. B., Watterson, I. G., Weaver, A. J., and Zhao, Z.-C.: Global climate projections, in: Climate Change 2007: The Physical Science Basis. Contribution of Working Group I to the Fourth Assessment Report of the Intergovernmental Panel on Climate Change, edited by: Solomon, S., Qin, D., Manning, M., Chen, Z., Marquis, M., Averyt, K. B., Tignor, M., and Miller, H. L., Cambridge University Press, Cambridge, UK and New York, NY, USA, 2007. 116

Meier, M. F., Dyurgerov, M. B., Rick, U. K., O'Neel, S., Pfeffer, W. T., Anderson, R. S., Anderson, S. P., and Glazovsky, A. F.: Glaciers dominate eustatic sea-level rise in the 21st century, Science, 317, 1064–1067, 2007. 116

Noël, B., Fettweis, X., van de Berg, W. J., van den Broeke, M. R., and Erpicum, M.: Sensitivity of Greenland Ice Sheet surface mass balance to perturbations in sea surface temperature and sea ice cover: a study with the regional climate model MAR, The Cryosphere, 8, 1871–1883, doi:10.5194/tc-8-1871-2014, 2014. 127

Radić, V. and Hock, R.: Regionally differentiated contribution of mountain glaciers and ice caps to future sea-level rise, Nat. Geosci., 4, 91–94, doi:10.1038/ngeo1052, 2011. 117

Radić, V., Bliss, A., Beedlow, A. C., Hock, R., Miles, E., and Cogley, J. G.: Regional and global projections of twenty-first century glacier mass changes in response to climate scenarios from global climate models, Clim. Dynam., 42, 37–58, doi:10.1007/s00382-013-1719-7, 2014. 117, 120, 121

Rignot, E., Velicogna, I., van den Broeke, M. R., Monaghan, A., and Lenaerts, J. T. M.: Acceleration of the contribution of the Greenland and Antarctic ice sheets to sea level rise, Geophys. Res. Lett., 38, L05503, doi:10.1029/2011GL046583, 2011. 116

TCD
9, 115–140, 2015

Rignot, E., Mouginot, J., Morlighem, M., Seroussi, H., and Scheuchl, B.: Widespread, rapid grounding line retreat of Pine Island, Thwaites, Smith, and Kohler glaciers, West Antarctica, from 1992 to 2011, Geophys. Res. Lett., 41, 3502–3509, doi:10.1002/2014GL060140, 2014. 116

Rogelj, J., Meinshausen, M., and Knutti, R.: Global warming under old and new scenarios using IPCC climate sensitivity range estimates, Nat. Clim. Change, 2, 248–253, doi:10.1038/nclimate1385, 2012. 122

Sakamoto, T. T., Komuro, Y., Nishimura, T., Ishii, M., Tatebe, H., Shiogama, H., Hasegawa, A., Toyoda, T., Mori, M., Suzuki, T., Imada, Y., Nozawa, T., Takata, K., Mochizuki, T., Ogochi, K., Emori, S., Hasumi, H., and Kimoto, M.: MIROC4h – a new high-resolution atmosphere–ocean coupled general circulation model, J. Meteorol. Soc. Jpn., 90, 325–359, doi:10.2151/jmsj.2012-301, 2012. 118

Shepherd, A., Ivins, E. R., A, G., Barletta, V. R., Bentley, M. J., Bettadpur, S., Briggs, K. H., Bromwich, D. H., Forsberg, R., Galin, N., Horwath, M., Jacobs, S., Joughin, I., King, M. A., Lenaerts, J. T. M., Li, J., Ligtenberg, S. R. M., Luckman, A., Luthcke, S. B., McMillan, M., Meister, R., Milne, G., Mouginot, J., Muir, A., Nicolas, J. P., Paden, J., Payne, A. J., Pritchard, H., Rignot, E., Rott, H., Sørensen, L. S., Scambos, T. A., Scheuchl, B., Schrama, E. J. O., Smith, B., Sundal, A. V., van Angelen, J. H., van de Berg, W. J., van den Broeke, M. R., Vaughan, D. G., Velicogna, I., Wahr, J., Whitehouse, P. L., Wingham, D. J., Yi, D., Young, D., and Zwally, H. J.: A reconciled estimate of of ice-sheet mass balance, Science, 338, 1183–1189, 2012. 116

Watanabe, M., Suzuki, T., O'ishi R., Komuro, Y., Watanabe, S., Emori, S., Takemura, T., Chikira, M., Ogura, T., Sekiguchi, M., Takata, K., Yamazaki, D., Yokohata, T., Nozawa, T., Hasumi, H., Tatebe, H., and Kimoto, M.: Improved climate simulation by MIROC5: mean states, variability, and climate sensitivity, J. Climate, 23, 6312–6335, 2010. 118

Zuo, Z. and Oerlemans, J.: Modelling albedo and specific balance of the Greenland ice sheet: calculations for the Søndre Strømfjord transect, J. Glaciol., 42, 305–317, 1996. 124

TCD
9, 115–140, 2015

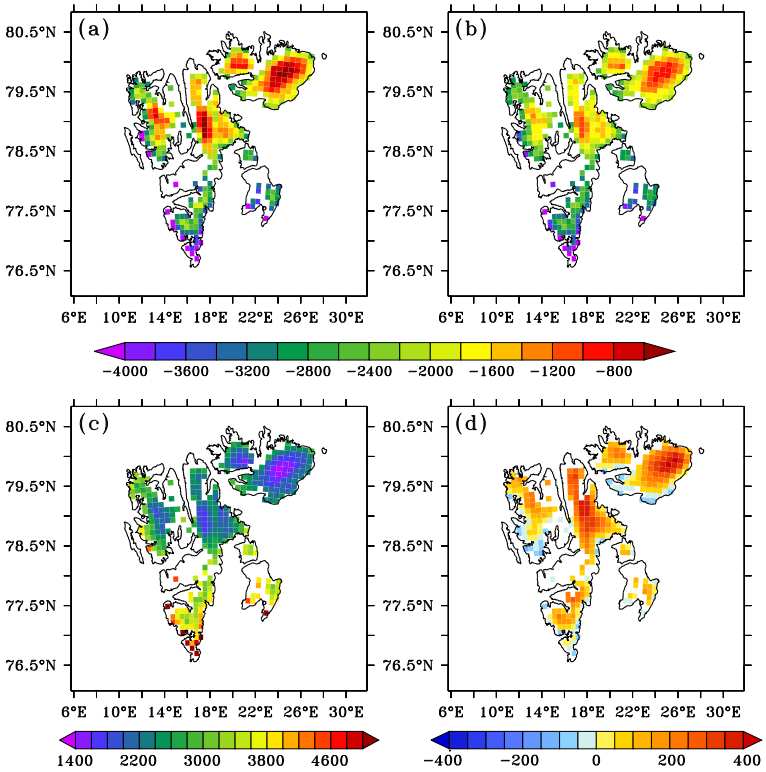

Figure 1. (a) 2070–2099 mean SMB (mm w.e. yr^{-1}) as simulated by MAR forced by the MIROC5-based RCP8.5 scenario. **(b)** Difference between **(a)** and the 1980–2005 mean shown in Lang et al. (2014) and in Supplement Fig. S1. **(c)** Same as **(b)** but for runoff. **(d)** Same as **(b)** but for precipitation.

TCD
9, 115–140, 2015

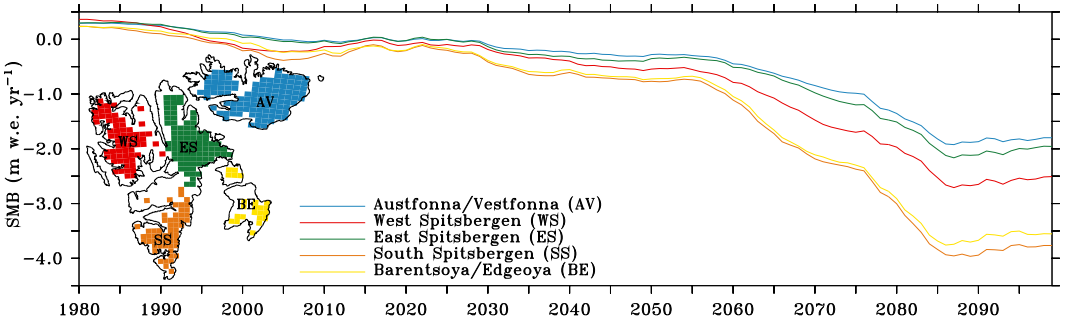

Figure 2. SMB 10-year running mean (m w.e. yr^{-1}) for 5 different regions (Austfonna and Vestfonna, west Spitsbergen, east Spitsbergen, south Spitsbergen and Barentsøya and Edgeøya) as simulated by MAR forced by the MIROC5-based historical scenario over 1980–2005 and RCP8.5 afterwards. The units are in m w.e. yr^{-1} (rather than Gt yr^{-1}) to be independent of different region areas. The permanent ice mask of each region defined for the regional evolution is shown in the inset.

TCD
9, 115–140, 2015

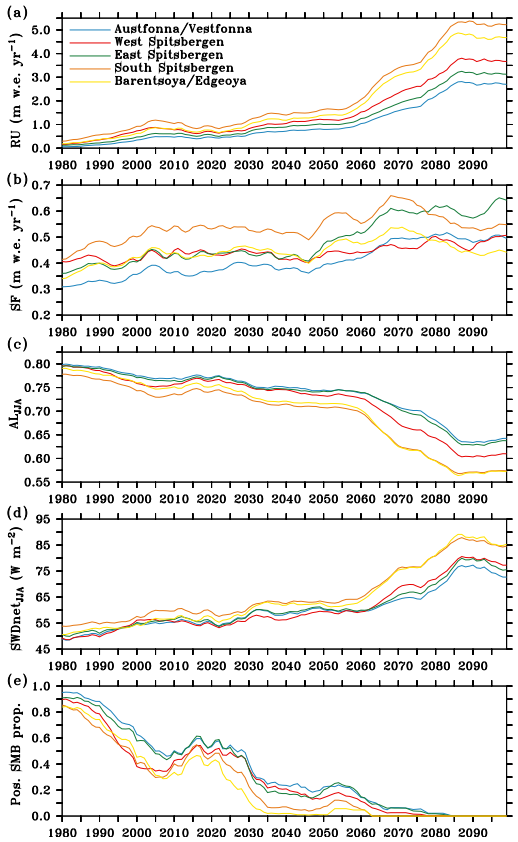

Figure 3. (a) Same as Fig. 2 but for the meltwater runoff (m w.e. yr^{-1}). **(b)** Same as **(a)** but for the snowfall (m w.e. yr^{-1}). **(c)** Same as **(a)** but for the JJA albedo. **(d)** Same as **(a)** but for the JJA net solar radiation absorbed by the surface (W m^{-2}). **(e)** Same as **(a)** but for the proportion of each region in the accumulation zone.

TCD
9, 115–140, 2015

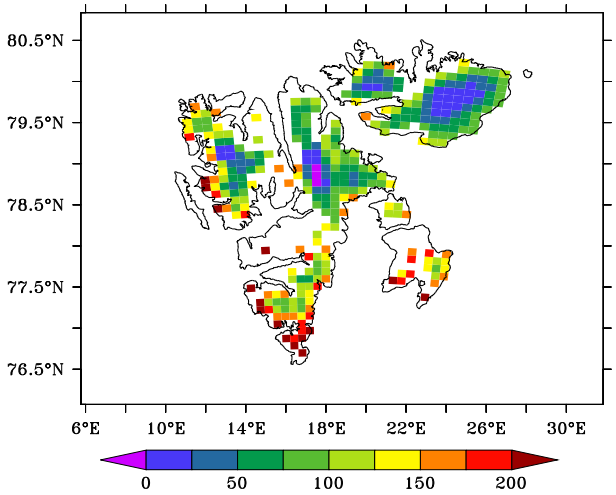

Figure 4. Projected anomaly of the cumulated surface ice loss (m) over 2006–2099 with respect to the 1980–2005 mean.

TCD
9, 115–140, 2015

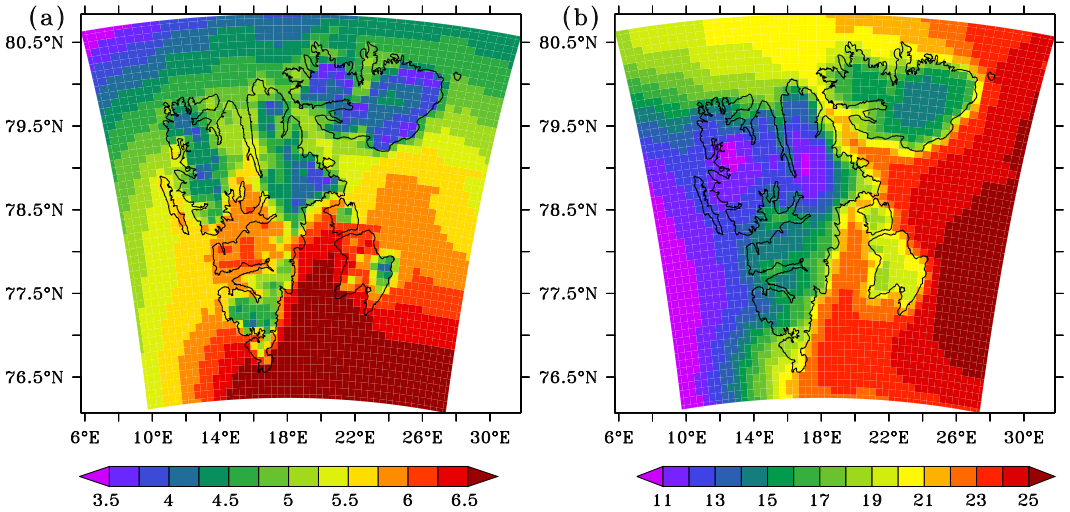

Figure 5. (a) 2070–2099 mean summer (JJA) near-surface temperature anomaly (°C) with respect to the 1980–2005 mean. **(b)** Same as **(a)** but for winter (DJF).

TCD
9, 115–140, 2015

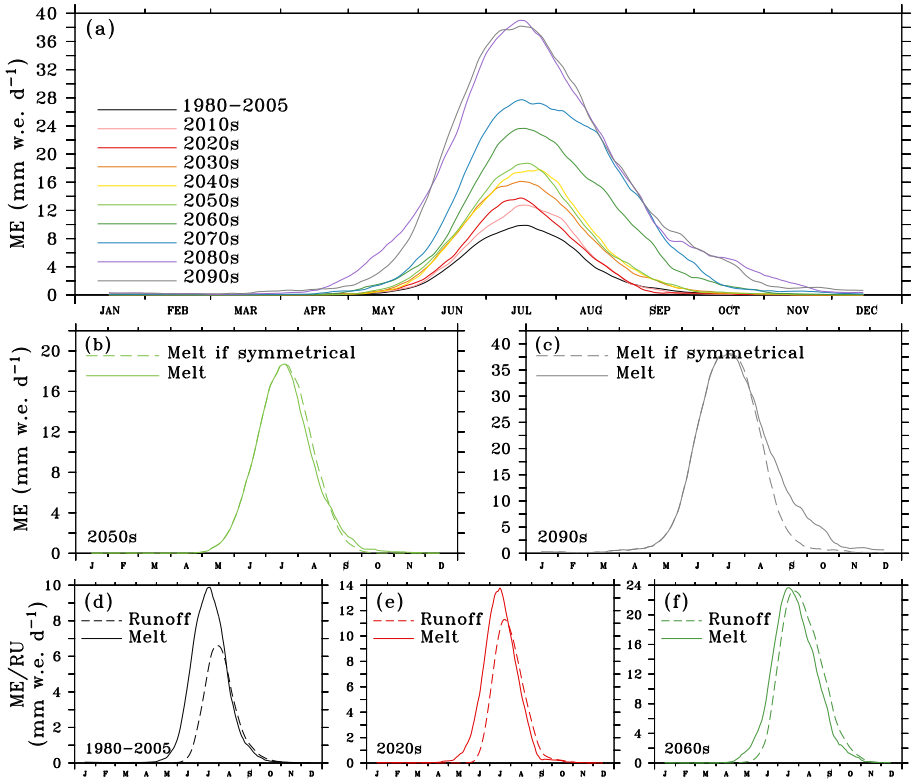

Figure 6. (a) Mean annual cycle of the surface melt (mm w.e. d^{-1}, 30-day running mean) for the listed decades. The 1980–2005 mean is shown in black as comparison. **(b)** Annual cycle of the surface melt in the 2050s (solid line) as well as, in dash, the cycle if it was symmetrical with respect to its maximum. **(c)** Same as **(b)** but for the 2090s. **(d)** Mean annual cycle of the melt (solid line) and runoff (dashed line) (mm w.e. d^{-1}) during the 1980–2005 period. **(e)** Same as **(d)** in the 2020s. **(f)** Same as **(d)** in the 2060s.

TCD
9, 115–140, 2015

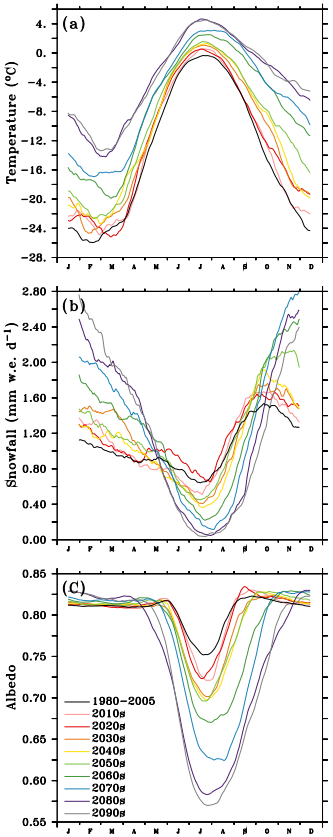

Figure 7. (a) Mean annual cycle of TAS (°C, 30-day running mean) over the permanent ice covered area for the listed decades. The 1980–2005 mean is given in black as comparison. **(b)** Same as **(a)** but for the snowfall (mm w.e. d^{-1}). As the daily variability of precipitation is very high, we have applied here a 60-day running mean instead of 30 days (like in Figs. 6 and 7a and c) in order to make the figure more clear. **(c)** Same as **(a)** but for the albedo.

TCD
9, 115–140, 2015

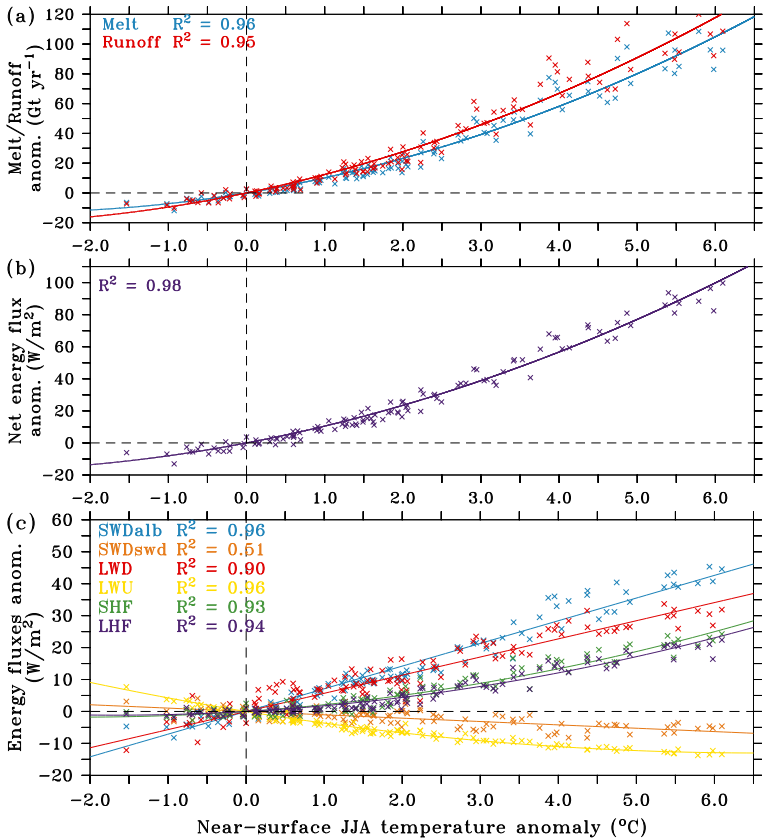

Figure 8. (a) Melt and runoff anomalies ($Gt\,yr^{-1}$) vs. TAS_{JJA} anomaly (°C). The anomalies are differences with respect to the 1980–2005 mean. **(b)** Same as **(a)** but for the JJA net energy flux at the surface ($W\,m^{-2}$). **(c)** Same as **(b)** but for the JJA energy balance components.

TCD
9, 115–140, 2015